Spreading of Intense Laser Beams Due to Filamentation

S. Wilks, P. E. Young, J. Hammer, M. Tabak, and W. L. Kruer
Lawrence Livermore National Laboratory, P.O. Box 5508, Livermore, California 94550
(Received 8 July 1994)

Channeling and filamentation of a laser beam is investigated experimentally and via computer simulations. A two-dimensional, fully nonlinear, fluid code has been developed and used to simulate the propagation of a laser pulse through an underdense plasma when $v_{osc}/v_e \sim 1$. Comparison to interferometrically measured density depressions shows good agreement. The limited axial extent of the density perturbation seen in experiment is linked by the simulation to filamentation and divergence of the laser beam. A characteristic angle of divergence of the laser beam is derived, and agreement is found with experiment and simulation.

PACS numbers: 52.35.Mw, 52.40.Db, 52.40.Nk, 52.65.+z

The filamentation of laser beams propagating through fully ionized plasmas has been extensively investigated, both theoretically [1–11] and experimentally [12–17], in recent years. This topic is of interest because it is widely thought that filamentation of laser beams can lead to degraded performance of inertial confinement fusion targets. More recently, the fast ignitor concept [18] has been proposed, which requires the propagation of a high intensity beam through an underdense plasma. Unfortunately, not only is filamentation difficult to observe experimentally, but the nonlinearly saturated state and its effect on laser propagation are poorly understood.

In this Letter, we first present the results of simulations of experiments in which a density channel is observed. The simulations quantitatively reproduce the experimental transverse plasma density profile and the limited axial extent of the density depression. The limited axial extent of the density depression results, in the simulation, from the fact that vigorous, nonlinear filamentation of the laser beam occurs at the end of a wide, ponderomotive pressure-induced plasma channel. It is found that the transverse plasma density perturbations created by the ponderomotive filamentation of the laser beam act as an ion grating with a characteristic wavelength, which causes the remainder of the beam to scatter off at a characteristic angle. An expression for this angle is derived and is verified by experimentally measuring the maximum deflection angle of the beam as a function of plasma density for a fixed laser intensity.

A typical plasma density channel can be seen in the interferogram of Fig. 1 (which was first shown in Ref. [14]). The background plasma was performed by a 1.064 μm wavelength laser pulse that irradiates a 0.5 μm thick target [parylene-$(CH)_n$] with an average intensity of 5×10^{13} W/cm^2. A second beam is delayed so that it interacts with an underdense, preformed plasma that has a parabolic density in the axial direction. The interaction beam has a wavelength of 1.064 μm, pulse width of 100 ps (FWHM), and is focused to a 50 μm $\times$ 350 μm line focus, using an $f/2$ lens and two cylindrical lenses with a peak intensity of 1.7×10^{15} W/cm^2. Nominal best focus is at the target plane. The resulting density depression, caused by the transverse ponderomotive force associated with the intensity gradient across the beam spot, is observed using interferometry. From the interferogram we find a peak density of $0.2n_c$ at the target plane, where n_c is the critical density at which the plasma frequency ω_{pe} equals the laser frequency ω_0 and a density gradient scale length $L_n = n_e^{-1}(dn_e/dx)^{-1} \sim 300$ μm. LASNEX simulations [19], concentrating just on the hydrodynamics of the exploding foil, were performed in order to determine the plasma parameters. These simulations predict a parabolic plasma, with peak density at the target plane, and an effective charge state Z of 3.5, as well as electron and ion temperatures of $T_e = 700$ eV and $T_i = 400$ eV, respectively.

The hydrodynamic simulation codes LASNEX [20] and a modified version of F3D [10] that includes nonlinear motion of the ions [21] are used to compare with the experimental results. For the propagation of the electromagnetic waves, LASNEX uses a ray trace and

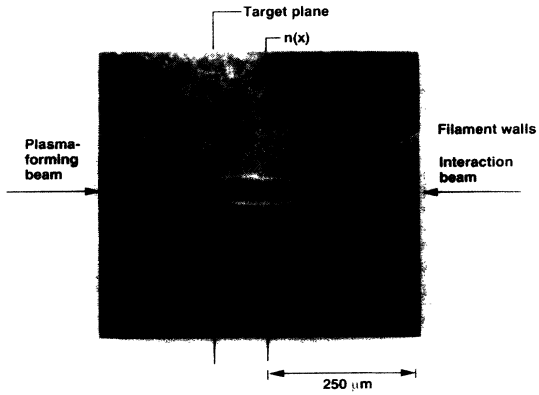

FIG. 1. Interferogram of an experiment in which a high intensity line focus interacts with a preformed plasma. The density perturbation produced by the beam can be seen, as can the walls, with density higher than the background density. These walls are formed as material is pushed out from the center of the ion channel.

 0031-9007/94/73(22)/2994(4)$06.00

geometrical optics approximation, while F3D solves an enhanced paraxial wave equation [22]. Thus, F3D is capable of modeling diffraction effects correctly, whereas LASNEX must approximate them by choosing a transverse grid size to be a wavelength of light. The ability of the codes to look at microscopic phenomena not readily diagnosed by experiment helped interpret some puzzles found in the experiment and suggested further experiments to understand this laser-plasma interaction.

We completed a series of simulations for the experiment associated with Fig. 1 using both codes. Only ponderomotive filamentation is included in the calculations, an assumption discussed below. Temperatures for the electrons and ions were held constant at 1 keV and 500 eV, respectively. (Note these are not exactly what LASNEX predicts, as LASNEX is only a guide of the temperatures in the experiment; we also expect some heating to occur during the interaction and have approximated the temperatures as given above.) No suprathermal electron effects are included, and laser absorption by inverse bremsstrahlung was turned off, in order to obtain similar results for both calculations. A spatially Gaussian (transverse full width at half maximum = 50 μm) laser pulse composed of 1000 parallel rays was used in LASNEX. Both nonlinear F3D and LASNEX used f/∞ beams for the calculations, a valid assumption to make since the Rayleigh length of the beam is approximately $\frac{1}{2}$ cm, and the interaction region is on the order of 500 μm. The y-z Cartesian geometry of the nonlinear version of F3D simulations approximated the fact that the laser was a line focus. LASNEX approximated this geometry (no variation in x) by simulating a thin annulus with r acting as y in r-z geometry. The laser was incident at $z = 0$. The material was 50% H, 50% C atomic fractions and remained fully ionized to good approximation ($Z = 3.5$) throughout the runs. The density profile for both codes was constant in y (transverse dimension) and parabolic in z (propagation direction) with peak $n_{\max} = 0.2n_c$ in the center of the simulation box (the density was $0.05n_c$ at the ends of the boxes). In addition, both nonlinear F3D and LASNEX found a dominant filament width of $10\lambda_0$, in agreement with Eq. (2) below.

Figure 2 shows the E-field contours of the laser, predicted by the nonlinear F3D code after 140 ps, near the peak of the laser pulse in the experiment. The remaining parameters were taken to be roughly those of the experiment and are well within error bars of the experiment. The depth of the channel at a point corresponding to the plane label $n(x)$ in Fig. 1, as inferred from the simulations, is approximately 10% of the background density. This is in excellent agreement with the channel depth measured from the experiment. A comparison of the transverse density profiles obtained from simulations and experiment is shown in Fig. 3. In fact, the 10% maximum density perturbation is nearly the value that one expects for the case where the transverse ponderomotive pressure

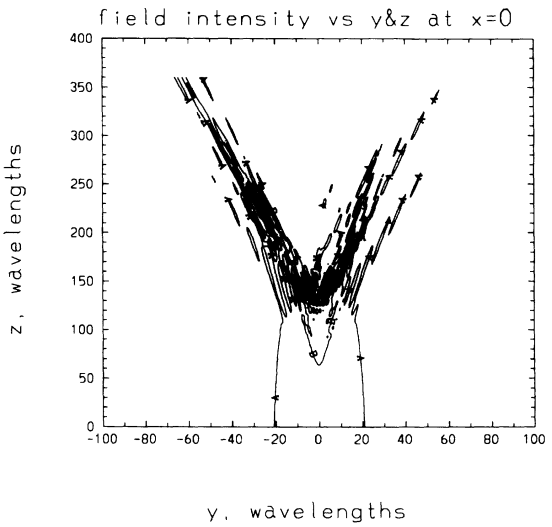

FIG. 2. E-field contours associated with the laser for a simulation done with parameters similar to the experiment in which interferogram of Fig. 1 was taken. Note the distinct angle at which laser light leaves the filamented region of light.

of the laser is made to adiabatically balance the thermal pressure of the plasma. This steady state is estimated as $\delta n/n_0 \approx \frac{1}{4}(v_{\rm osc}/v_e)^2 \approx 16\%$, in rough agreement with experiment and theory. In the calculations presented here we have assumed, for simplicity, ponderomotive effects only. For the 2×10^{15} W/cm^2 case, this is a marginal assumption. Theory using nonlocal electron transport [9] predicts that the growth length for thermal filamentation is about the same as that for ponderomotive filamentation, although we point out that the thermal filamentation length should be increased since $v_{\rm osc}/v_e \sim 1$. For the higher intensity cases discussed below, ponderomotive filamentation clearly dominates. However, for the cases described here, the LASNEX simulations showed that including thermal effects did not alter the results significantly.

Perhaps the most striking feature of the interferogram in Fig. 1 is the fact that the density channel disappears

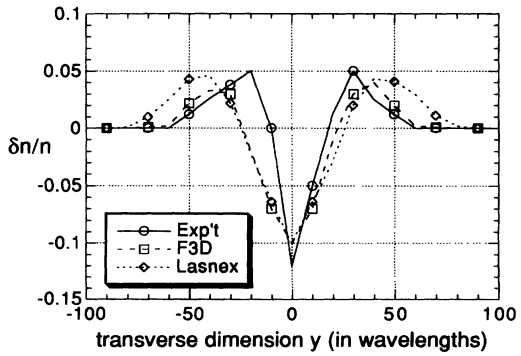

FIG. 3. Transverse profile of ion density taken at plane marked $n(x)$ in Fig. 1, for experiment and the two hydrocodes.

near the peak of the density profile, located at the target plane. From Fig. 2 (note that the peak of the density profile is located at $z = 180\lambda_0$), we see that the simulation shows the channel terminating at roughly the density seen in the experiment, i.e., near $n = 0.18n_c$. Again, this is roughly the point at which we predict a large growth rate for the ponderomotive filamentation instability. At this point, all along the transverse cross section of the line focus, the beam would break up into small filaments that are randomly oriented. The fine scale density perturbations that these filaments produce will no longer result in a coherent density depression. In fact, the simulations show strong transverse modulation of the ion density, where are associated with these filaments. This would not be observed by the interferometry technique used. Therefore, this process of filamentation at the end of the density channel would explain the sudden disappearance of the ponderomotively created density depression associated with the 50 μm width of the laser beam as seen in the experiment. It should be pointed out that once filamentation occurs, both codes give the envelope of the forward-directed light cone at roughly the same angle.

One way of understanding this beam spreading mechanism is to look at the dispersion relation for ponderomotive filamentation [5], and solve, not for k as usual, but for the angle θ between the scattered light waves (k_s) and the incident wave (k_0). Using the approximation of small angle scattering, we find that the real component of the k associated with the ion perturbation is $k_r \approx k_0\theta$. Replacing this in the dispersion relation in Ref. [5], and noting that growth will be maximized when $\partial k_i/\partial\theta = 0$, we obtain

$$\theta \approx \frac{1}{2}\left(\frac{v_{\rm osc}}{v_e}\right)\left(\frac{\omega_{pe}}{\omega_0}\right). \quad (1)$$

The most unstable wave number is still given by $k_\perp^{\rm max}$,

$$k_\perp^{\rm max} = \frac{1 v_{\rm osc}\omega_{pe}\omega_0}{2 v_e \omega_0 c}, \quad (2)$$

which for the parameters of the experiment, varies from $0.09\omega_0/c$ to $0.2\omega_0/c$, corresponding to wavelengths of $11\lambda_0$ and $5\lambda_0$, respectively. For the parameters of the experiment, if we assume that the filamentation is occurring around $0.18n_c$, then θ should be about 0.2 rad. From the nonlinear F3D runs, we measure $0.175 \leq \theta \leq 0.225$ rad, and from the LASNEX runs, we obtain about $0.2 \leq \theta \leq 0.25$ rad. The definition of the maximum angle is not precise, but the dependence of the trends on laser intensity and plasma density have been verified. This relation has been shown to hold for a number of simulations in this parameter regime.

An alternative way of understanding this spreading mechanism is via refraction from the unstable transverse ion density modulations. These density perturbations saturate at some significant level as the laser light propagates into this region. Now the light no longer sees a homogeneous transverse plasma, but one with large ion density perturbations at the most unstable wave number for the instability. The light then refracts out of the channel at a characteristic angle, given by Eq. (1).

This theory, which predicts that the light will scatter from the filamented region with a specific scaling of density and intensity given by Eq. (1), has been confirmed in a second series of experiments. We have measured the angular distribution of the light transmitted through an underdense plasma by placing Tri-X film (which is filtered by 2 mm thick RG 1000 glass to pass 1.06 μm laser light [23]) around the collecting lens for the interaction beam. The interaction beam in this case was focused to a circular spot by an $f/2$ lens to peak intensities from 2.5×10^{16} to 5×10^{16} W/cm^2. The Rayleigh length here is only 500 μm, but the longitudinal point at which the beam filaments is much further (~200 μm from the peak density). The larger the angle of deflection of the light, the more the film around the collecting lens was exposed. Figure 4 shows film exposures of a number of interactions, corresponding to increasing peak plasma densities, keeping laser parameters constant. Figure 5 shows the deflection angle as a function of peak plasma density, for a number of experiments, compared to what theory predicts. Note that changing the incident intensity of the interaction beam also changes the deflection angle as predicted by Eq. (1). Interferograms still show a sudden disappearance of the ion channel at a point just in front of the peak density, consistent with the interpretations given above. Note that for the intensities accessed in these experiments, $k_{\rm max}$ is of order ω_{pe}/c. For much weaker intensities, θ may be an underestimate, since the most unstable filaments can nonlinearly evolve to a shorter wavelength than that predicted by Eq. (2). In addition, when the light pressure greatly exceeds the plasma pressure, we expect a nearly evacuated channel to form, after a very short transient of this beam spreading behavior. However, this regime is still under investigation.

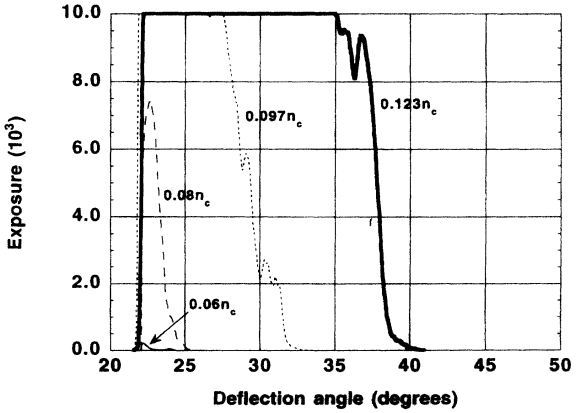

FIG. 4. Lineouts of the film that was placed around the collecting lens, showing increasing deflection angle of line with increasing density.

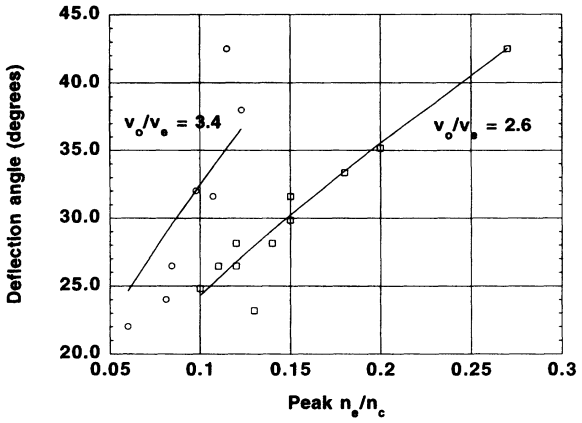

FIG. 5. Experimentally measured deflection angle versus n_{peak}/n_c. The solid line is the theoretically expected deflection angle, given by Eq. (1).

Clearly, the filamentation does not necessarily have to be ponderomotive. This was simply chosen to compare with experiment and just provides a well defined ion grating to be set up in the plasma, where subsequent laser light can interact with it. Similar effects take place for parameters where the ion fluctuations are driven by thermal filamentation. The only change would be that the unstable wave numbers would be associated with thermal filamentation. The fact that a filamented laser beam can deflect at a considerable angle is of importance to applications that require a significant fraction of the laser energy to be placed in a narrow, well known spot. Additionally, a proper energy balance in an experiment where this effect is thought to take place would necessarily require measurement of light scattered outside the collecting lenses.

The observation of an ion channel in an underdense plasma created by an intense laser beam has been observed both in experiment and simulation. The explanation for the sudden disappearance of the channel before the laser has propagated through the peak density has been attributed to filament formation, followed by a deflection of the laser light from the ion perturbations. This deflection of light was observed both in experiment and in simulations and agrees with a simple estimate for the deflection angle.

We thank Dr. J. Woodworth, Dr. G. Guethlein, Dr. J. Moody, and Dr. M. D. Perry for useful discussions on this work. We also thank the authors of Ref. [10] and C. H. Still for developing the F3D code. Finally, we thank R. Gonzales, G. London, and W. Cowens for operating the laser during the experiment. This work was performed under the auspices of the U.S. Department of Energy by the Lawrence Livermore National Laboratory under Contract No. W-7405-Eng-48.

[1] P. K. Kaw, G. Schmidt, and T. W. Wilcox, Phys. Fluids **16**, 1522 (1973).
[2] F. W. Perkins and E. J. Valeo, Phys. Rev. Lett. **32**, 1234 (1974).
[3] C. E. Max, Phys. Fluids **19**, 74 (1976).
[4] D. Anderson and M. Bonnedal, Phys. Fluids **25**, 105 (1979).
[5] W. L. Kruer, Comments Plasma Phys. Controlled Fusion **9**, 63 (1985). The dispersion relation for filamentation we use here can be found on page 67.
[6] K. Estabrook, W. L. Kruer, and D. S. Bailey, Phys. Fluids **28**, 19 (1985).
[7] E. P. Liang and A. B. Langdon, Phys. Fluids **30**, 175 (1987).
[8] A. J. Schmidt, Phys. Fluids **31**, 3079 (1988); A. J. Schmidt, Phys. Fluids B **3**, 186 (1991).
[9] E. M. Epperlein, Phys. Rev. Lett. **65**, 2145 (1990).
[10] R. L. Berger, B. F. Lasinski, T. B. Kaiser, E. A. Williams, A. B. Langdon, and B. I. Cohen, Phys. Fluids B **5**, 2243 (1993).
[11] R. Rankin, C. E. Capjack, and C. R. James, Phys. Rev. Lett. **63**, 1597 (1989).
[12] P. E. Young, H. A. Baldis, R. P. Drake, E. M. Campbell, and K. G. Estabrook, Phys. Rev. Lett. **61**, 2336 (1988).
[13] P. E. Young, H. A. Baldis, T. W. Johnston, W. L. Kruer, and K. G. Estabrook, Phys. Rev. Lett. **63**, 2812 (1989); **65**, 2145 (1990); E. M. Epperlein, Phys. Fluids B **1**, 3082 (1991).
[14] P. E. Young, Phys. Fluids B **3**, 2331 (1991).
[15] O. Willi, T. Afshar-rad, S. E. Coe, and A. Giulietti, Phys. Fluids B **2**, 1318 (1990); T. Afshar-rad, S. E. Coe, O. Willi, and M. Desselberger, Phys. Fluids B **4**, 1301 (1992).
[16] O. Willi and P. Lee, Opt. Commun. **55**, 120 (1985).
[17] C. Joshi, C. E. Clayton, A. Yasuda, and F. F. Chen, J. Appl. Phys. **47**, 1318 (1982).
[18] M. Tabak, J. Hammer, M. E. Glinsky, W. L. Kruer, S. C. Wilks, J. Woodworth, E. M. Campbell, and M. D. Perry, Phys. Plasmas **1**, 1626 (1994).
[19] K. Estabrook (private communication).
[20] G. D. Zimmerman and W. L. Kruer, Comments Plasma Phys. Controlled Fusion **2**, 51 (1975).
[21] S. C. Wilks *et al.*, Bull. Am. Phys. Soc. **38**, 1935 (1993).
[22] M. D. Feit and J. A. Fleck, Jr., J. Opt. Soc. Am. B **5**, 633 (1988).
[23] P. E. Young and K. Estabrook, Phys. Rev. E **49**, 5556 (1994).

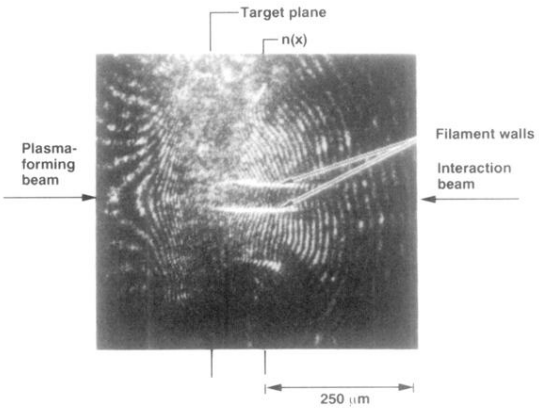

FIG. 1. Interferogram of an experiment in which a high intensity line focus interacts with a preformed plasma. The density perturbation produced by the beam can be seen, as can the walls, with density higher than the background density. These walls are formed as material is pushed out from the center of the ion channel.